Modelling and Experimental Investigation of Carangiform Locomotion for Control

Scott D. Kelly Richard J. Mason
Carl T. Anhalt Richard M. Murray Joel W. Burdick
Division of Engineering and Applied Science
California Institute of Technology
Pasadena, CA 91125

September 15, 1997

Submitted, 1998 American Control Conference

Abstract

We propose a model for planar carangiform swimming based on conservative equations for the interaction of a rigid body and an incompressible fluid. We account for the generation of thrust due to vortex shedding through controlled coupling terms. We investigate the correct form of this coupling experimentally with a robotic propulsor, comparing its observed behavior with that predicted by unsteady hydrodynamics. Our analysis of thrust generation by an oscillating hydrofoil allows us to characterize and evaluate certain families of gaits. Our final swimming model takes the form of a control-affine nonlinear system.

1 Introduction and perspective

Certain fish and marine mammals are arguably superior to man-made aquatic propulsors in speed, efficiency, maneuverability, and/or stealth [10]. Recent efforts to realize pisciform robots have earned celebrity focusing on biomimetic design [13]. Parallel efforts to model flapping-foil propulsion in a fashion compatible with control theory [2] have set the stage for a comprehensive mathematical treatment of pisciform locomotion. Of particular interest to design engineers are "carangiform" members of the fish order Percomorphi. The term, introduced by Breder [1], applies to members of the family Carangidae and other fish exhibiting similar body morphology and propulsive efficiency [7]. It is our goal to model the essential features of carangiform swimming in a manner consistent in perspective with both modern mechanics and nonlinear control.

Our investigation of carangiform swimming fits within a broader program directed at the anaysis and control of robotic locomotion [5, 6]. Our perspective is geometric; we regard each internal configuration of a robotic propulsor with a point in an appropriate *shape manifold*, and equate the cyclic deformations which provide propulsion with closed curves therein. A particular time-parametrized, cyclic deformation is said to define a *gait*. The set of all time parametrizations of a particular loop in shape space constitutes an equivalence class of gaits.

The role of fluid viscosity in carangiform swimming is twofold. Clearly, it accounts for the dissipation of energy from the swimmer-fluid system. More subtly, however, it is the nonzero viscosity of water which resolves D'Alembert's paradox in an aquatic setting and permits the generation of thrust due to circulation about control surfaces. We regard the caudal fin of a carangiform swimmer as a hydrofoil. The shedding of vorticity from its trailing edge induces a net circulation about the fin's perimeter and a hydrodynamic lift which is conveyed as thrust to the swimmer's body.

For the present paper, we choose to neglect certain dissipative phenomena inherent to viscous fluids. It is our hope that conservative models can accurately predict at least the short-time motion of streamlined bodies through relatively inviscid media. The mechanism by which vorticity is shed, however, is as ubiquitous among fluids of nonzero viscosity as it is important. If we are to adopt a Lagrangian point of view, we must alter any model which we derive to incorporate the generation of thrust by vortex shedding.

The caudal fins of nature's fastest carangiform swimmers are often lunate in profile. The vortex structures which evolve around fins of this sort are essentially three-dimensional. The mechanism by which thrust is developed by such a fin, however, is apparent in any cross-section perpendicular to the profile. For simplicity's sake, we focus in this paper on planar carangiform locomotion through incompressible fluids.

In Section 2, we propose a simple model for the planar propulsion of a rigid body coupled to a small hydrofoil. This model is based largely on elementary hydrodynamics, but requires the more involved modelling of the generation of thrust and the shedding of vorticity on the foil itself. In Section 3, we describe an experimental investigation of the self-propulsion of a flapping foil. Our laboratory apparatus affords us both the quantitative assessment of various two-input gaits and the visualization of the fluid flow around a swimming foil. We compare data from our experiment with the predictions of a simulation based on unsteady hydrodynamics in Section 4. Our simulation allows us to classify certain gaits according to their geometric properties; we explain the relationships among their observed characteristics and the elements of our model. We demonstrate in Section 5 that our swimming model takes the form of a control-affine system with drift, and propose in Section 6 an approach to its control analysis.

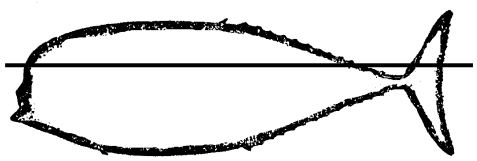

Figure 1: The separation of body and caudal fin in a section of a louvar

2 Planar carangiform locomotion

An essential feature of carangiform propulsion is the localization of vortex shedding to the trailing edge of the caudal fin of the propulsor. Vorticity is shed there in accordance with a Kutta condition; we will sometimes refer to the trailing point of a planar caudal fin as a Kutta point. In constructing a model for carangiform locomotion which addresses the dynamics of both propulsor and fluid, we begin with the interaction of the propulsor's body with the fluid in the large. Neglecting the dissipative effect of the fluid's viscosity, we may treat the fluid as inviscid away from the Kutta point.

We borrow the notion of a *substitution vortex* from [8]. It is demonstrated therein that the flow around an aerofoil resembles, to a good approximation at distances greater than one chord length from the aerofoil's center, the flow around an appropriately located point vortex. The strength of this vortex corresponds to the circulation about the aerofoil. Figure 1 depicts the silhouette of a louvar — a representative carangiform swimmer. We have marked a cross-section away from the midline of the fish; insofar as it affects the animal's body in the plane of this section, the flow about the caudal fin resembles that due to a point vortex with time-varying strength. As circulation is developed about the fin due to vortex shedding at the Kutta point, it experiences a force analogous to aerodynamic lift. This force is transferred to the body through the caudal peduncle. The narrowness of the carangid's caudal peduncle justifies its absence from a representative horizontal section, and therefore its absence from our planar model. Our prototypical planar carangid is depicted in Figures 2 and 3. By varying the position x_{T} and the angle β, the swimmer in Figure 2 controls the effective velocity and angle of attack of the caudal fin. This, in turn, dictates the circulation about the fin and the hydrodynamic lift it experiences. In essence, then, the swimmer controls the position x_v and strength Γ of the substitution vortex, as in Figure 3.

We define two frames of reference. We denote spatial position with respect to the first, a fixed "laboratory" frame, by the coordinates (x^1, x^2). We denote position with respect to the second, fixed in the body, by the coordinates (y^1, y^2). We will sometimes abuse notation by using the symbol x to denote abstract position. Let $\mathcal{B}$ denote the region occupied by the body of the propulsor, $\mathcal{F}$ the region occupied by the fluid, and $\mathcal{S}$ the surface separating the two.

With respect to the stationary frame, the fluid velocity field $u(x,t)$ on $\mathcal{F}$

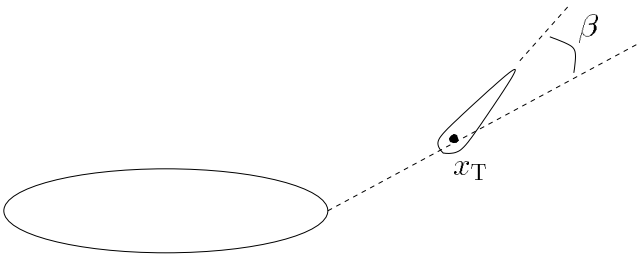

Figure 2: The prototypical planar carangid

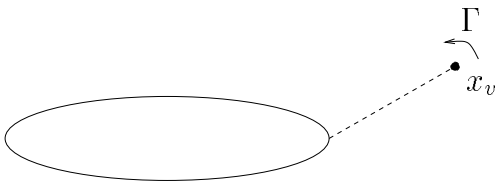

Figure 3: Substitution vortex model

satisfies Euler's equation

$$\frac{\partial u}{\partial t} + \mathcal{P}(u \cdot \nabla u) = 0, \tag{1}$$

where the symbol $\mathcal{P}$ denotes the Hodge projection onto that component of its argument which is solenoidal and parallel to $\mathcal{S}$ on $\mathcal{S}$. Equation (1) is often written in terms of the *pressure gradient*

$$\nabla p = -\mathcal{G}(u \cdot \nabla u) = -\big(u \cdot \nabla u - \mathcal{P}(u \cdot \nabla u)\big).$$

Since the pressure $p(x,t)$ will itself appear nowhere in our final equations, we avoid introducing unnecessary symbols here.

Taking the curl of (1), we obtain Helmholtz's vorticity equation

$$\frac{\partial \zeta}{\partial t} + u \cdot \nabla \zeta = \zeta \cdot \nabla u, \tag{2}$$

where $\zeta(x,t) = \nabla \times u(x,t)$ is the vorticity field on $\mathcal{S}$. It is to the planar form of this equation that a forcing term is most easily added to represent local vortex shedding. If x_{K} denotes the spatial position of a point at which vorticity is shed and $\dot{\Gamma}$ the rate at which shedding occurs, the scalar vorticity field $\zeta(x,t)$ must satisfy

$$\frac{\partial \zeta}{\partial t} + u \cdot \nabla \zeta = \zeta \cdot \nabla u + \dot{\Gamma}\delta(x_{\mathrm{K}}), \tag{3}$$

where $\delta(\cdot)$ denotes a Dirac delta function. The subscript K is intended to suggest that vorticity is shed in accordance with a Kutta condition. If the symbol Γ

is to represent a circulation, we must assign units of inverse length squared to the delta function. Indeed, the circulation $\Gamma(t)$ about an aerofoil which sheds vorticity from a single Kutta point varies at precisely the rate of shedding in this sense.

In taking the curl of (1), we surrender some knowledge of the flow field. Solutions to the elliptic boundary-value problem which recaptures $u(x,t)$ from $\zeta(x,t)$ are only unique up to an additive gradient vector field. Taking the gradient projection of (1), then, we obtain the additional equation

$$\frac{\partial}{\partial t}\mathcal{G}u = 0. \tag{4}$$

In what follows, we make repeated use of the identity

$$\begin{aligned}\int_{\mathcal{F}} \nabla\cdot(\phi v)dA &= \int_{\mathcal{F}} \phi\nabla\cdot v dA + \int_{\mathcal{F}} v\cdot\nabla\phi dA \\ &= \int_{\mathcal{S}} \phi v\cdot n dS,\end{aligned}$$

where v is a vector field on $\mathcal{F}$, ϕ a real-valued function on $\mathcal{F}$, and n the outward-pointing unit vector normal to the surface S. We denote the mass of the body by m, its moment of inertia about its center of mass by I, and the laboratory position of its center of mass by $(x^1_{\rm cm}, x^2_{\rm cm})$. We fix the origin of the coordinate system (y^1, y^2) to this point; we denote the inclination of the y^1-axis with respect to the x^1-axis by θ. We denote the fluid density by ρ.

The net pressure force on the body in the x^i direction is given, at any moment, by

$$\begin{aligned}F_{x^i} &= -\int_{\mathcal{S}} p(x) n\cdot e_{x^i} dS \\ &= -\int_{\mathcal{F}} e_{x^i}\cdot\nabla p\, dA,\end{aligned} \tag{5}$$

where e_{x^i} denotes the unit vector in the x^i direction. The net pressure moment about the body's center of mass is given by

$$\begin{aligned}M &= \int_{\mathcal{S}} p(x)(n^1 y^2 - n^2 y^1) dS \\ &= \int_{\mathcal{S}} p(x)(y^2, -y^1)\cdot(n^1, n^2) dS \\ &= \int_{\mathcal{F}} (y^2, -y^1)\cdot\nabla p\, dA.\end{aligned} \tag{6}$$

We define the vector $y^\perp = (y^2, -y^1)$ for each position vector $y = (y^1, y^2) \in \mathbb{R}^2$.

We denote the position of the substitution vortex in the laboratory and body-fixed frames by x_v and y_v, respectively. As it moves with velocity $\dot{x}_v$ in the

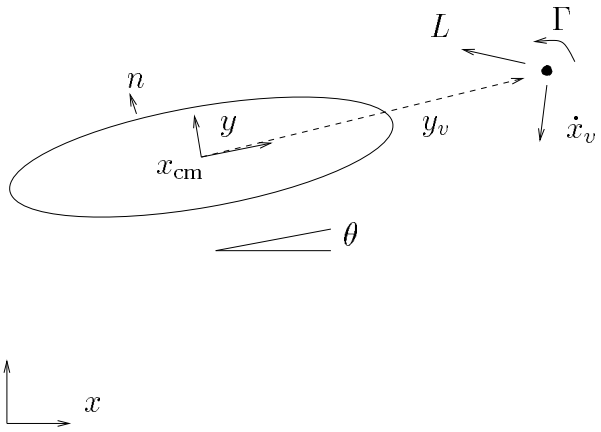

Figure 4: Forces and moments on the carangid

former, it observes an instantaneous ambient flow velocity of $U_v = u(x_v) - \dot{x}_v$. The resulting lift force is given by

$$L(t) = \rho U_v(t) \times e_3 \Gamma(t),$$

where L and U_v are regarded as vectors in $\mathbb{R}^3$ and e_3 refers to the unit vector determining right-handed coordinates from (x^1, x^2) or (y^1, y^2). The lift L is transferred to the body in addition to the moment

$$T(t) = y_v(t) \times L(t)$$

about its center of mass. We obey tradition in regarding the velocity $u(x_v)$ to be the velocity which would be be measured at the point x_v in the absence of the singularity there.

The complete situation is depicted in Figure 4. It follows that the motion of the body through the fluid is governed by the equations

$$\begin{aligned}
m\ddot{x}^1_{\mathrm{cm}} &= \int_{\mathcal{F}} e_{x^1} \cdot \mathcal{G}(u \cdot \nabla u) dA + \rho \Gamma (u(x_v) - \dot{x}_v)_{x^2}; \\
m\ddot{x}^2_{\mathrm{cm}} &= \int_{\mathcal{F}} e_{x^2} \cdot \mathcal{G}(u \cdot \nabla u) dA - \rho \Gamma (u(x_v) - \dot{x}_v)_{x^1}; \\
I\ddot{\theta} &= -\int_{\mathcal{F}} y^{\perp} \cdot \mathcal{G}(u \cdot \nabla u) dA - \rho \Gamma (y^1_v (u(x_v) - \dot{x}_v)_{y^1} + y^2_v (u(x_v) - \dot{x}_v)_{y^2})
\end{aligned} \tag{7}$$

together with (3) and (4). It is worth noting that these equations may, in the absence of the substitution vortex, be derived via Lagrangian reduction from canonical Euler-Lagrange equations on $T(\mathrm{SE}(2) \times \mathrm{Diff}_{\mathrm{vol}}(\mathcal{F}))$, where the latter term in the Cartesian product refers to the manifold of volume-preserving diffeomorphisms of the region occupied by the fluid. The authors present this point of view in a forthcoming publication.

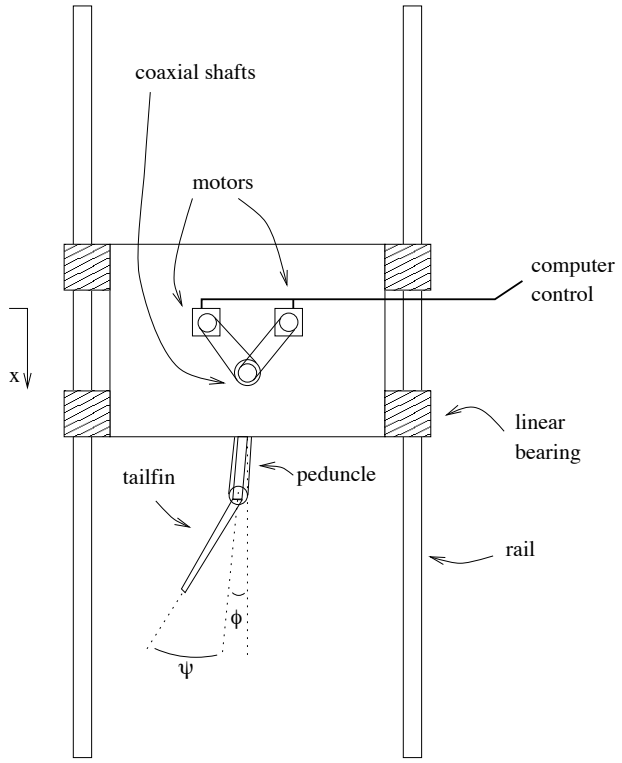

Figure 5: The apparatus from the top

3 Experimental apparatus

We have yet to relate changes in the position and orientation of the caudal fin to changes in the position and strength of the substitution vortex. Equivalently, we have yet to model the development of hydrodynamic lift by a moving fin. For the present paper, we demonstrate the validity of a particular model for the forward propulsion of a rectilinearly constrained flapping-foil device.

Figures 5 and 6 depict our experimental apparatus from the top and side, respectively. The actuated mechanism is intended to exemplify the hind section of a planar carangiform swimmer, and is suspended from a carriage which is free to translate along the two-meter length of our laboratory water tank. The apparatus permits independent, software-based control of the horizontal angles ϕ and ψ between the direction of translation, a narrow peduncle, and a fin as deep as the water in the tank. A Polhemus sensor is mounted to the carriage, and continuously returns its measured displacement. A 0.2 % solution of commercially available Kalliroscope fluid provides opacity and reflectivity to the water in the tank, allowing us to photograph patterns of flow with ordinary cameras and lighting.

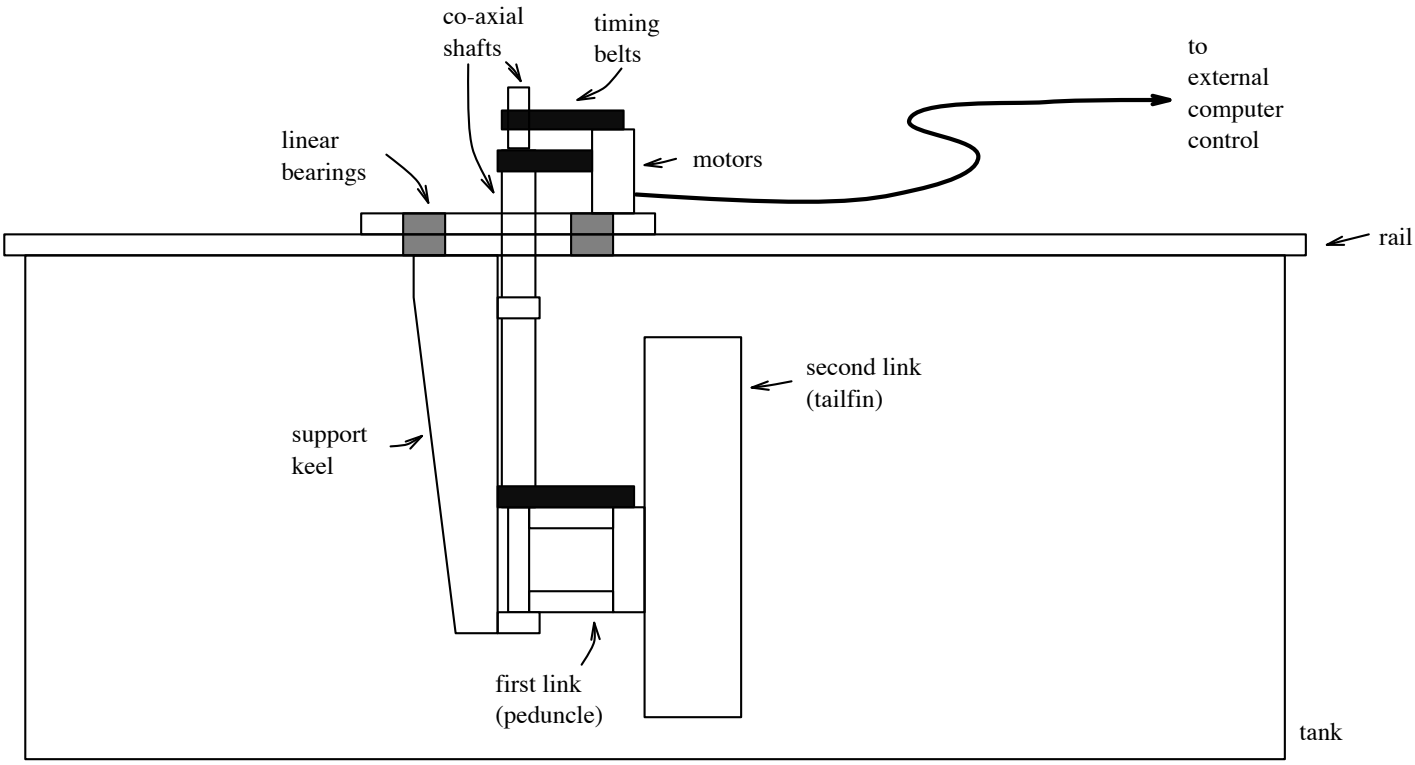

Figure 6: The apparatus from the side

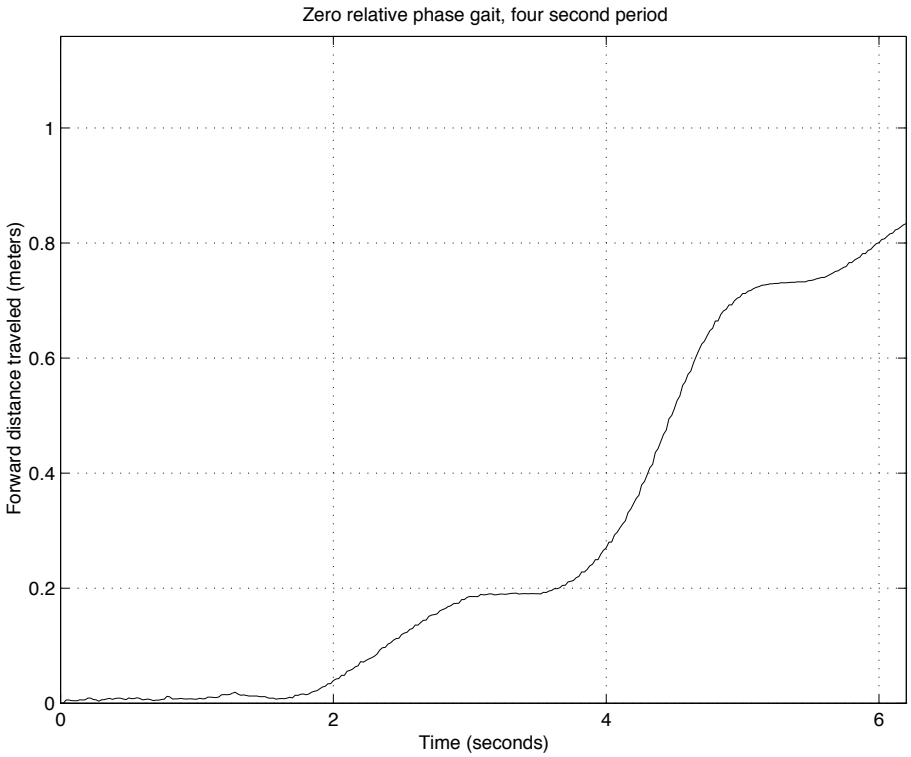

Figure 7: Measured distance versus time with the peduncle and fin aligned

We have collected data representing over two hundred gaits, varying the amplitude and frequency of sinusoidal variations in the peduncle and fin angles and the relative phase between them. Figures 7 and 8 show the measured displacement and velocity as functions of time for a gait characterized by the alignment of the fin and peduncle. We present the measured displacement versus time for a gait more reminiscent of those favored by biological carangids alongside a graph predicted computationally in Section 4.

4 Simulation and Validation

We use two-dimensional thin-aerofoil theory to derive a model for the force acting on the caudal fin; we are guided in part by the similar approach taken in [2]. Throughout the remainder of this section, we imagine the fin to propel a body with (apparent) mass m in the direction x. In reality, the body of a swimming carangid is subject to hydrodynamic drag; we denote the associated drag coefficient by k_d. The lifting force per span on a steadily translating and pitching foil with chord length c, translational velocity U, and angle of attack

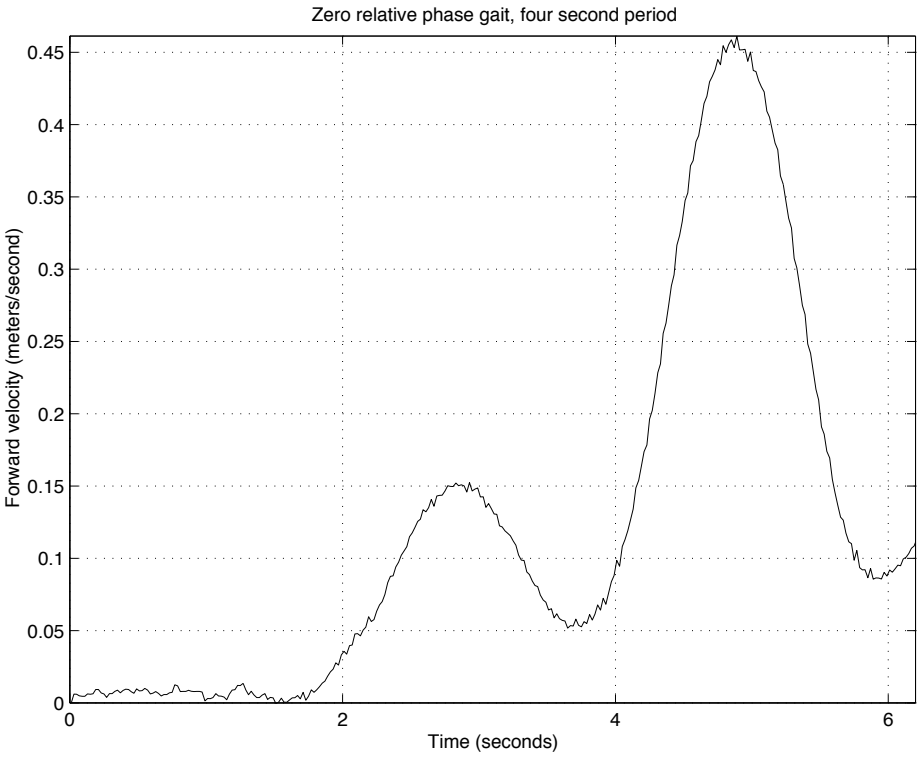

Figure 8: Measured velocity versus time with the peduncle and fin aligned

α in an ideal fluid of density ρ is given by

$$L = \pi\rho c U^2[A_0 + \frac{A_1}{2}],$$

where, for a flat plate at low angles of attack,

$$A_0 = \alpha + \frac{c}{U}\dot{\alpha}(\frac{1}{2} - h)$$

and

$$A_1 = \frac{c}{2U}\dot{\alpha}.$$

The symbol h refers to the fractional chord length between the leading edge and the pitch axis. In our case, we take $h = 0$ for forward swimming and $h = 1$ for backward swimming. In the unsteady case where $U(t)$ and $\dot{\alpha}(t)$ become time-varying, as long as the reduced frequency (rate of rotation times chord length divided by $U(t)$) is not too large, we can modify the expression for lift as follows [4]:

$$L(t) = \pi\rho c\left[U^2(t)A_0(t) + \frac{3c}{4}\frac{\partial}{\partial t}\left(U(t)A_0(t)\right) + U^2(t)\frac{A_1(t)}{2} + \frac{c}{4}\frac{\partial}{\partial t}\left(U(t)A_1(t)\right)\right].$$

Substituting in the above expressions for $A_0(t)$ and $A_1(t)$, we obtain

$$L(t) = \pi\rho c\left[U^2(t)\alpha(t) + (\frac{3}{2} - h)cU(t)\dot{\alpha}(t) + c^2(\frac{1}{2} - \frac{3h}{4})\ddot{\alpha}(t) + \frac{3c}{4}\dot{U}(t)\alpha(t)\right]. \tag{8}$$

The quantities $U(t)$ and $\alpha(t)$ may be expressed in terms of the position and joint angle variables x, ϕ, and ψ thus:

$$U = \left[(-\dot{x} + l_{\text{ped}}\sin(\phi)\dot{\phi})^2 + (l_{\text{ped}}\cos(\phi)\dot{\phi})^2\right]^{1/2}$$

$$\alpha = \arctan(\frac{-l_{\text{ped}}\cos(\phi)\dot{\phi}}{-\dot{x} + l_{\text{ped}}\sin(\phi)\dot{\phi}}) - (\phi + \psi).$$

Care must be taken to properly interpret α and its derivatives when the foil moves backward through the fluid, and the edge normally thought of as the trailing edge of the foil becomes the leading edge. We find the lift force as a function of x, ϕ, and ψ and their derivatives to second order, neglecting higher-order derivatives. This lift force acts perpendicularly to the instantaneous velocity vector of the fin; the component T of the lift in the longitudinal direction x results in an acceleration of the body $\ddot{x}$. Meanwhile, the body is also assumed

to experience a drag force D proportional to $\dot{x}^2$. We neglect drag forces on the fin as distinct from the general drag term, and write

$$T = -L\sin(\arctan(\frac{-l_{\rm ped}\cos(\phi)\dot{\phi}}{-\dot{x} + l_{\rm ped}\sin(\phi)\dot{\phi}})),$$

$$D = -\rho\kappa_d\dot{x}^2\ \mathrm{sign}(\dot{x}),$$

and

$$\ddot{x} = \frac{1}{m}(T + D). \tag{9}$$

Here κ_d is the drag coefficient alluded to earlier. In (8), every term other than the leading term in the expression for lift implicitly contains $\ddot{x}$, so $\ddot{x}$ appears implicitly on the right hand side of (9) as well as on the left. When constructing a simulation, we must therefore employ an iterative procedure to find the correct $\ddot{x}$ at each time step.

In the present simulation we consider only forces resulting directly from the motion of the foil, and neglect wake effects which depend on the time history of the motion. This is one promising area for future refinement of the model. Based on the analyses in [12] and [3] of a similar problem involving a foil which pitches and heaves laterally, we anticipate that the effect of the wake will be to attenuate and introduce a phase lag to the quasi-steady part of the lift. The wake has little effect, however, at low reduced frequencies.

In both simulation and experiment, we focus our attention on gaits with joint angle trajectories of the form:

$$\begin{aligned} \phi &= A\sin(\omega t) \\ \phi + \psi &= B\cos(\omega t). \end{aligned}$$

We make no claim that gaits of this type represent any particular performance optimum in the large set of imaginable joint angle trajectories. They have the virtue of simplicity, however, and recall the swimming of biological carangids.

Simulation reveals that many gaits of the above form will drive the body either forward or backward once an initial velocity in the appropriate direction is established. However, for any given gait there is an interesting distinction between the two directions, which we can best illustrate by suppressing the empirical drag term D.

For a particular gait, there will be one direction of travel in which the lateral motion of the leading edge of the foil precedes the lateral motion of the trailing edge of the foil. This will be the forward or $-x$ direction of motion for a gait of the above form with amplitudes A and B of different sign; it will be the backward direction of motion for a gait with A and B of the same sign. In this direction of travel, the fish will tend to accelerate or decelerate to a steady-state longitudinal velocity $\dot{x}_{\rm SS}$ and remain in a neighborhood of that velocity (with small oscillations in $\dot{x}$ of period $(2\pi/\omega)$. In other words, the gait has a limited

steady-state velocity in this direction even in the absence of drag. On the other hand, if the body moves with the same gait but with the sign of $\dot{x}$ reversed, then the lateral motion of the new leading edge (formerly trailing edge) lags the lateral motion of the trailing edge (formerly leading edge). In this direction of motion, the longitudinal velocity of the body will tend to increase exponentially without any limit in the absence of drag. Naturally, drag forces will impose some steady-state limit in reality.

The reason for this discrepancy in behaviour can be seen by considering the way in which the quasi-steady part of the lift generates thrust. In order to generate propulsive thrust in the right direction, the angle between the foil and the centerline must always be smaller in magnitude than, or of sign opposite to that of, the angle between the instantaneous velocity of the foil and the centerline. If the lateral motion of the leading edge precedes the lateral motion of the trailing edge, then as the longitudinal velocity grows large and the instantaneous velocity vector tends toward the centerline, the gait must begin at some point to generate thrust in the wrong direction. When the counter-productive thrust generated over a single period equals the amount of thrust in the right direction, the body settles into a steady cycle with constant mean velocity. This is illustrated in Figure 9. On the other hand, if the lateral motion of the leading edge lags that of the trailing edge, the foil need never generate any counter-productive thrust, and the body can accelerate indefinitely (in the absence of drag).

Since the latter sort of gait comes without a built-in "speed limit," one might ask why it is not used more by real carangiform fish, who are generally observed to move the leading edge of the tail sideways in advance of the trailing edge [7]. One answer is that, because the non-speed-limited gaits involve larger angles of attack than the speed-limited gaits, a non-speed-limited gait will cause the foil to stall or otherwise violate the assumptions of our model, especially at low to moderate longitudinal speeds. We speculate that a swimming robot or fish will find it necessary to use a speed-limited gait at low speeds, but might later make the transition to a non-speed-limited gait. This kind of behavior would provide a role for feedback control based on the measured surrounding fluid flow, in contrast with the kind of open-loop joint trajectories described above.

When we compare the results of computer simulation to data from the physical apparatus, we find that the model is less realistic at low longitudinal speeds. It tends to overpredict thrust at these speeds, suggesting that the apparatus will accelerate from rest to a steady state more quickly than it does in reality. However, the model does appear to do a good job of predicting the steady-state motion of the system, as illustrated in Figure 10. It is not really surprising, given the assumptions of small reduced frequency underlying it, that our model should be more successful at higher velocities and give poor results when the body is near rest.

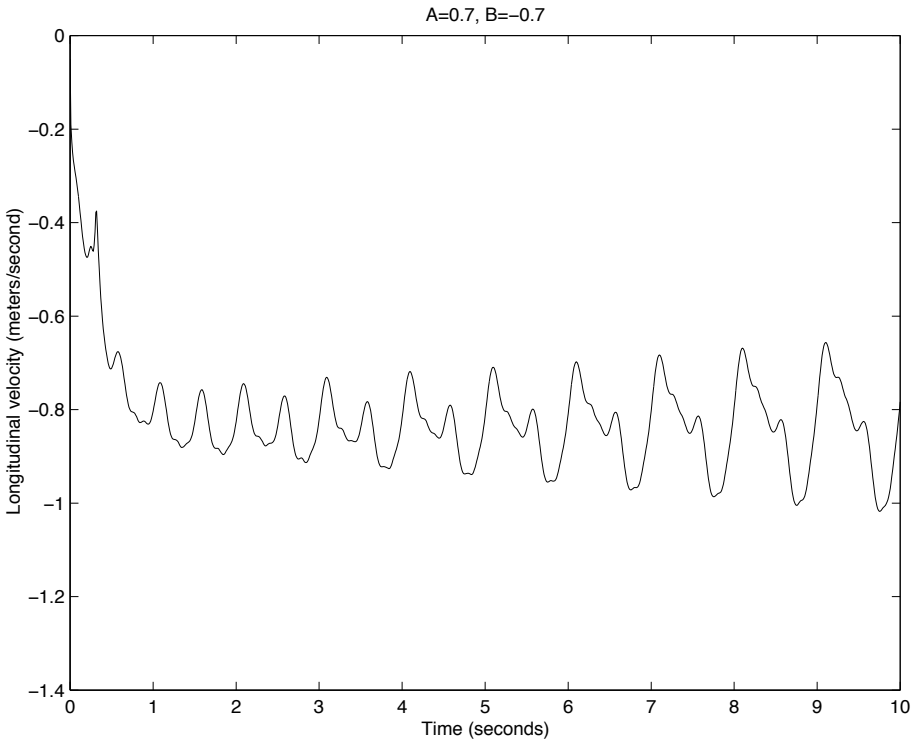

Figure 9: Oscillation about a steady state velocity for $\phi = 0.7\sin(2\pi t)$ and $\phi + \psi = -0.7\cos(2\pi t)$

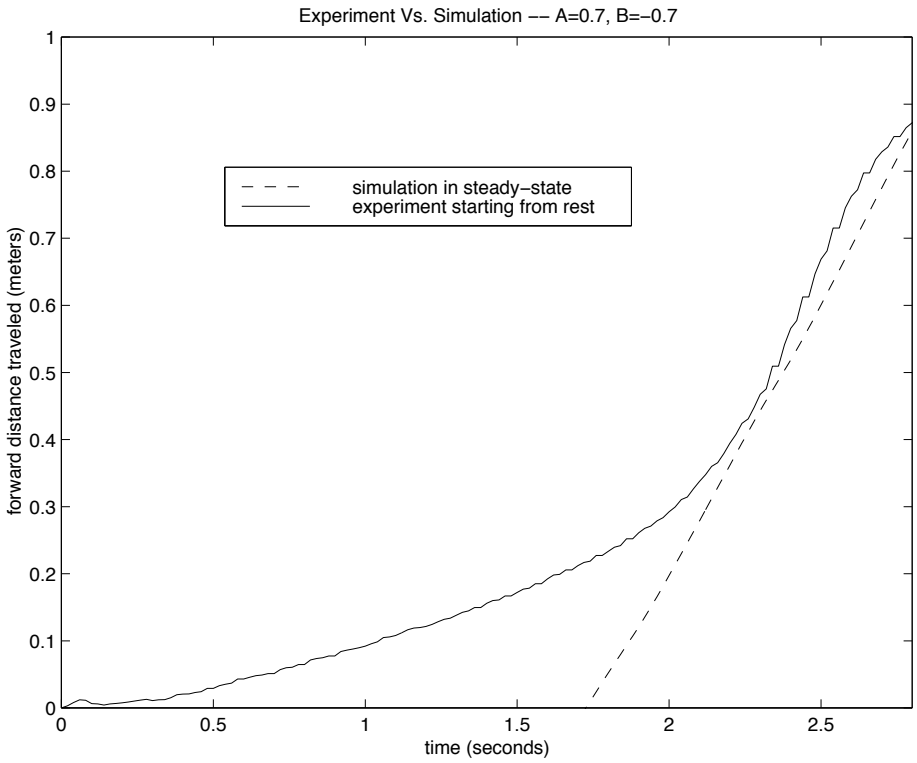

Figure 10: Simulated and observed displacement for $\phi = 0.7\sin(2\pi t)$ and $\phi+\psi = -0.7\cos(2\pi t)$

5 The model as a control system

We now express the equations from Section 2 as a control system. We treat as inputs τ^i the quantities $\dot{x}_v^1$, $\dot{x}_v^2$, and $\dot{\Gamma}$. In practice, we are likely to influence y_v rather than x_v directly, and input controls at the level of accelerations, but these represent simple and obfuscating algebraic adjustments. Though the experimental apparatus described in Section 3 permits only two controls, it is easy to imagine a practical pisciform robot with additional articulation. Furthermore, though the hydrofoil model developed in Section 4 includes nonlinear terms which involve higher time-derivatives of ϕ, ψ, and x_{cm}, these nonlinearities take significant effect only when the system is near rest. Combining (3), (4), and (7), we write

$$\frac{d}{dt}\begin{bmatrix} x_v^1 \\ x_v^2 \\ \Gamma \\ x_{\text{cm}}^1 \\ \dot{x}_{\text{cm}}^1 \\ x_{\text{cm}}^2 \\ \dot{x}_{\text{cm}}^2 \\ \theta \\ \dot{\theta} \\ \mathcal{G}u(x,t) \\ \zeta(x,t) \end{bmatrix} = [f] + \begin{bmatrix} 1 \\ 0 \\ 0 \\ 0 \\ 0 \\ 0 \\ \rho\Gamma/m \\ 0 \\ (\rho\Gamma/I)(y_v^1\cos\theta - y_v^2\sin\theta) \\ 0 \\ 0 \end{bmatrix}\tau^1 + \begin{bmatrix} 0 \\ 1 \\ 0 \\ 0 \\ -\rho\Gamma/m \\ 0 \\ 0 \\ 0 \\ (\rho\Gamma/I)(y_v^1\sin\theta + y_v^2\cos\theta) \\ 0 \\ 0 \end{bmatrix}\tau^2 + \begin{bmatrix} 0 \\ 0 \\ 1 \\ 0 \\ 0 \\ 0 \\ 0 \\ 0 \\ 0 \\ 0 \\ \delta(x_v) \end{bmatrix}\tau^3, \tag{10}$$

where

$$[f] = \begin{bmatrix} 0 \\ 0 \\ 0 \\ \dot{x}_{\text{cm}}^1 \\ \frac{1}{m}\left(\int_{\mathcal{F}} e_{x^1}\cdot\mathcal{G}(u\cdot\nabla u)dA + \rho\Gamma u(x_v)\cdot e_{x^2}\right) \\ \dot{x}_{\text{cm}}^2 \\ \frac{1}{m}\left(\int_{\mathcal{F}} e_{x^2}\cdot\mathcal{G}(u\cdot\nabla u)dA - \rho\Gamma u(x_v)\cdot e_{x^1}\right) \\ \dot{\theta} \\ \frac{1}{I}\left(-\int_{\mathcal{F}} y^\perp\cdot\mathcal{G}(u\cdot\nabla u)dA - \rho\Gamma u(x_v)\cdot(y_v^1 e_{y^1} + y_v^2 e_{y^2})\right) \\ 0 \\ \zeta\cdot\nabla u - u\cdot\nabla\zeta \end{bmatrix}.$$

Recall that $\mathcal{P}u(x,t)$ is determined by $\zeta(x,t)$, and that $u(x,t) = \mathcal{P}u(x,t) + \mathcal{G}u(x,t)$; it follows that the above system of equations is in standard control-affine form.

6 Future work

A task immediately at hand is the control analysis of (10). In practice, our control efforts target only the variables $x^i_{\rm cm}$ and θ and (perhaps) their time derivatives; we do not care how the fluid evolves per se. We recall a notion of projected accessibility from [5], defined in reference to the generic nonlinear system with drift

$$\dot{q} = f(q) + h_1(q)\tau^1 + \cdots + h_m(q)\tau^m, \tag{11}$$

where $q \in Q$. We define the accessibility algebra $\mathfrak{C}$ to be the smallest subalgebra of $\mathfrak{X}(Q)$ containing $f, h_1, \ldots, h_m$. The accessibility distribution C on Q is then defined by

$$C(q) = \text{span}\{X(q) | X \in \mathfrak{C}\}, \quad q \in Q.$$

It is shown in [11] that the system (11) is locally accessible if $\dim C(q) = \dim T_q Q$ for all $q \in Q$.

Now suppose $Q = Q_1 \times Q_2$, and let $\pi : Q \to Q_1$ and $T\pi : TQ \to TQ_1$ denote the projection onto the first component of Q and its tangent map, respectively. Define the *restricted accessibility distribution* $T\pi C$ at $q_1 \in Q_1$ by

$$T\pi C(q_1) = \text{span}\{T\pi X(q) | X \in \mathfrak{C}, q_1 = \pi(q)\}.$$

If $\dim T\pi C(q_1) = \dim T_{q_1} Q_1$ for all $q_1 \in Q$, we will refer to (11) as *locally* Q_1 *accessible*. Loosely speaking, this property corresponds to accessibility of the system on Q_1 without regard for the evolution of the system on Q_2. Clearly, if the system on $Q_1 \times Q_2$ is locally accessible, it is locally Q_1 accessible.

In the present setting, we are interested in the TSE(2) controllability of the system (10) on $\mathbb{R}^3 \times T\text{SE}(2) \times \mathfrak{X}_G(\mathcal{F}) \times \mathfrak{X}_S(\mathcal{F})$, where the latter symbols refer to the spaces of gradient vector fields on $\mathcal{F}$ and solenoidal vector fields on $\mathcal{F}$ which are parallel to $\mathcal{S}$ on $\mathcal{S}$, respectively. Computing the system's TSE(2) accessibility will be the first step toward a determination of the desired controllability.

Though the generic model proposed in Sections 2 and 5 is amenable to fully planar locomotion, we have only verified the hydrofoil model from Section 4 in a restricted setting. The experimental apparatus described in Section 3 constrains the point about which the peduncle pivots to move rectilinearly. We are presently constructing an apparatus which will provide complete planar mobility to our robotic propulsor.

The continuous acceleration observed for some simulated gaits is nonphysical, an artifact of our neglecting the dissipative effects of fluid viscosity. The inclusion of dissipation will improve both our hydrofoil model and our more abstract swimming model, and we intend to pursue its integration into both. In the former case, we expect to capture dissipative drag with a nonzero drag coefficient k_d. In the latter, we may introduce viscous dissipation to (3) as it is added to (2) to obtain the compatibility equation

$$\frac{\partial \zeta}{\partial t} + u \cdot \nabla \zeta = \zeta \cdot \nabla u + \nu \nabla^2 \zeta.$$

Here ν represents the kinematic viscosity [9].

7 Acknowledgements

The authors would like to thank Fong Liu for his assistance in the design and construction of the experimental apparatus and Professor Ted Wu for his encouragement and the use of his laboratory. Funding for this research was provided by the Office of Naval Research through the STTR program. Additional funding for Scott Kelly's research was provided in part by NSF grant CMS-9502224, and in part by an ONR Graduate Fellowship.

References

[1] C. M. Breder. The locomotion of fishes. *Zoologica*, 4:159–297, 1926.

[2] Karen A. Harper, Matthew D. Berkemeier, and Sheryl Grace. Modeling the dynamics of spring-driven, oscillating-foil propulsion. Submitted to the IEEE Journal of Oceanic Engineering.

[3] T. Von Karman and W. R. Sears. Airfoil theory for non-uniform motion. *Journal of the Aeronautical Sciences*, 5(10):379–390, 1938.

[4] Joseph Katz and Allen Plotkin. *Low Speed Aerodynamics: From Wing Theory to Panel Methods*. McGraw-Hill, Inc., 1991.

[5] Scott D. Kelly and Richard M. Murray. Geometric phases and robotic locomotion. *Journal of Robotic Systems*, 12:417–431, 1995. Extended version available online via http://avalon.caltech.edu/cds/reports.

[6] Scott D. Kelly and Richard M. Murray. The geometry and control of dissipative systems. In *Proc. IEEE Control and Decision Conference*, Kobe, Japan, 1996.

[7] Sir James Lighthill. *Mathematical Biofluiddynamics*. SIAM, 1975.

[8] L. M. Milne-Thomson. *Theoretical Aerodynamics*. Dover, 1973.

[9] L. M. Milne-Thomson. *Theoretical Hydrodynamics*. Dover, 1996.

[10] J. N. Newman and T. Y. Wu. Hydromechanical aspects of fish swimming. In Theodore Y. T. Wu, Charles J. Brokaw, and Christopher Brennen, editors, *Swimming and Flying in Nature*, pages 615–634, 1974.

[11] H. Nijmeijer and A. J. van der Schaft. *Nonlinear Dynamical Control Systems*. Springer-Verlag, New York, 1990.

[12] T. Theodorsen. General theory of aerodynamic instability and the mechanism of flutter. Technical report, NACA Report 496, 1935.

[13] M. S. Triantafyllou and G. S. Triantafyllou. An efficient swimming machine. *Scientific American*, 272:64–70, 1995.